Compact Resolved Ejecta in the Nearest Tidal Disruption Event

Perlman, Eric S.; Meyer, Eileen T.; Wang, Q. Daniel; Yuan, Qiang; Henriksen, Richard; Irwin, Judith; Krause, Marita; Wiegert, Theresa; Murphy, Eric J.; Heald, George

Published in:
The Astrophysical Journal

DOI:
10.3847/1538-4357/aa71b1

Publication date:
2017

The Astrophysical Journal, 842:126 (9pp), 2017 June 20 https://doi.org/10.3847/1538-4357/aa71b1

Compact Resolved Ejecta in the Nearest Tidal Disruption Event

Eric S. Perlman[1], Eileen T. Meyer[2], Q. Daniel Wang[3], Qiang Yuan[3,4], Richard Henriksen[5], Judith Irwin[5], Marita Krause[6], Theresa Wiegert[5], Eric J. Murphy[7], George Heald[8,9], and Ralf-Jürgen Dettmar[10]
[1] Department of Physics and Space Sciences, Florida Institute of Technology, 150 W. University Boulevard, Melbourne, FL 32901, USA
[2] Department of Physics, University of Maryland—Baltimore County, 1000 Hilltop Circle, Baltimore, MD 21250, USA
[3] Department of Astronomy, University of Massachusetts, LGRT-B 619E, 710 North Pleasant Street, Amherst, MA 01003-9305, USA
[4] Purple Mountain Observatory, Chinese Academy of Sciences, no. 2 West Beijing Road, Nanjing, Jiansu 210008, China
[5] Department of Physics, Engineering Physics & Astronomy, Queens University, Kingston, Ontario, K7L 3N6, Canada
[6] Max-Planck Institut für Radioastronomie, Auf dem Hügel 69, D-53121, Bonn, Germany
[7] US Planck Data Center, The California Institute of Technology, MC 220-6, Pasadena, CA 91125, USA
[8] CSIRO Astronomy and Space Science, 26 Dick Perry Avenue, Kensington WA 6151, Australia
[9] Kapteyn Astronomical Institute, P.O. Box 800, 9700 AV, Groningen, The Netherlands
[10] Astronomical Institute, Faculty for Physics and Astronomy, Ruhr-Universität Bochum, D-44780 Bochum, Germany
Received 2017 February 6; revised 2017 May 2; accepted 2017 May 6; published 2017 June 22

Abstract

Tidal disruption events (TDEs) occur when a star or substellar object passes close enough to a galaxy's supermassive black hole to be disrupted by tidal forces. NGC 4845 ($d = 17$ Mpc) was host to a TDE, IGR J12580 +0134, detected in 2010 November. Its proximity offers us a unique close-up of the TDE and its aftermath. We discuss new Very Long Baseline Array (VLBA) and Karl G. Jansky Very Large Array observations, which show that the radio flux from the active nucleus created by the TDE has decayed in a manner consistent with predictions from a jet-circumnuclear medium interaction model. This model explains the source's broadband spectral evolution, which shows a spectral peak that has moved from the submillimeter (at the end of 2010) to GHz radio frequencies (in 2011–2013) to <1 GHz in 2015. The milliarcsecond-scale core is circularly polarized at 1.5 GHz but not at 5 GHz, consistent with the model. The VLBA images show a complex structure at 1.5 GHz that includes an east–west extension that is ∼40 mas (3 pc) long, as well as a resolved component that is 52 mas (4.1 pc) northwest of the flat-spectrum core, which is all that can be seen at 5 GHz. If ejected in 2010, the northwest component must have had $v = 0.96c$ over five years. However, this is unlikely, as our model suggests strong deceleration to speeds $<0.5c$ within months and a much smaller, sub-parsec size. In this interpretation, the northwest component could have either a non-nuclear origin or be from an earlier event.

Key words: galaxies: active – galaxies: individual (NGC 4845) – galaxies: nuclei – radio continuum: galaxies

1. Introduction

A star or substellar object will be partially or fully tidally disrupted when it passes close enough by a supermassive black hole (SMBH). Such tidal disruption events (TDEs) are expected to occur every 10^3–10^5 years for a typical galaxy (Magorrian & Tremaine 1999; Wang & Merritt 2004). This rate could be substantially higher (as high as once every few years), if the SMBH has a companion that is either an intermediate-mass black hole or SMBH (e.g., Chen et al. 2009). The debris of the disrupted object will be accreted onto the black hole, producing flaring emission at X-ray, ultraviolet, and optical wavelengths. A typical $t^{-5/3}$ behavior of the X-ray luminosity, following the decrease of the fallback rate of the debris, is a distinctive feature of TDEs (Phinney 1989). Jets can also be launched by such an event. When they interact with the circumnuclear medium (CNM) high-energy particle acceleration could occur. Observations show that at least some TDEs do launch relativistic jets. Sw J1644+57 (full name Swift J164449.3+573451, $z = 0.3534$; Bloom et al. 2011; Burrows et al. 2011; Levan et al. 2011; Zauderer et al. 2011) and Sw J2058+05 ($z = 1.1853$; Cenko et al. 2012) are examples, exhibiting super-Eddington X-ray emission and a long-lasting radio emission expected to arise from the jet-CNM interaction. Detailed modeling of both events suggests that the jets were moving along our lines of sight. It is then natural to expect that there should be more events with off-axis jets.

IGR J12580+0134 was a TDE detected in the nucleus of NGC 4845—a galaxy located in the Virgo cluster, at a distance of only ∼17 Mpc. Due to its proximity, IGR 1258+0134 gives a rare chance to scrutinize a TDE and its aftermath with the highest possible resolution. The source was initially detected in 2010 November by *Integral* (Walter et al. 2011). Follow-up X-ray observations with *XMM-Newton*, *Swift,* and *MAXI*, together with *Integral* data, suggest that the source probably resulted from a TDE of a super-Jupiter by the galaxy's central SMBH (Nikolajuk & Walter 2013). Spectral fitting to the *XMM-Newton* data indicates a soft X-ray excess (with temperature 0.33 keV) above the power law (with index $\Gamma \simeq 2.2$) from the TDE, likely representing the collective emission from unrelated discrete sources and/or truly diffuse hot plasma because of the completely different absorption compared with that of the TDE (Nikolajuk & Walter 2013).

The radio counterpart of the TDE was detected serendipitously in 2011 December by the Jansky Very Large Array (JVLA)[11] in a nearby galaxy survey (CHANG-ES; Irwin et al. 2015) where the core was a factor of 10 brighter than seen in *FIRST* observations conducted between 1993 and 2004. The radio spectrum, peaking at GHz frequencies, and its variation suggest self-absorbed synchrotron emission with changing optical thickness. These phenomena can be naturally explained by an expanding radio

[11] The National Radio Astronomy Observatory and Long Baseline Observatory are facilities of the National Science Foundation operated under cooperative agreement by Associated Universities, Inc.

Table 1
Radio Interferometry Observations

Observation				rms Noise, μJy beam^{-1}			
Date (Epoch)	Array and Config.	ν (GHz)	Beam Size (PA), arcsec	I	Q	U	V
1995 Feb 27	VLA/D (NVSS)	1.4	45 × 45(0)	450	⋯	⋯	⋯
1997 Aug 21, 25	VLA/C	8.4	7.08 × 5.69(64.51)	100	⋯	⋯	⋯
1998 Oct 09	VLA/B (FIRST)	1.4351	6.4 × 5.4(0)	150	⋯	⋯	⋯
2011 Dec 19 (T1)	VLA/D	5.99833	10.98 × 9.06(−1.40)	15	15	15	12
2011 Dec 30 (T1)	VLA/D	1.57470	38.58 × 34.27(−5.22)	40	27	27	28
2012 Feb 23, 25 (T2)	VLA/C	5.99854	3.05 × 2.75(−11.71)	3.9	3.2	3.2	3.3
2012 Mar 30 (T2)	VLA/C	1.57484	12.18 × 11.10(−41.76)	45	19	19	26
2012 Jun 11 (T3)	VLA/B	1.57499	3.51 × 3.33(22.69)	18	15	15	15
2015 Jun 22, 26 (T4)	VLA/A	1.5195	1.73 × 1.06(43.27)	88	58	58	59
2015 Jun 22, 26 (T4)	VLA/A	5.499	0.47 × 0.33(46.20)	13	16	17	16
2015 Oct 08	VLBA	1.5474	9.26[a] × 3.71[a] (−2.83)	128	48	46	124
2015 Oct 08	VLBA	4.9795	2.91[a] × 1.19[a] (−0.52)	55	37	40	35

Note.
[a] Milliarcseconds.

lobe, powered by the jet injection of the TDE. A moderately relativistic jet model fits the original radio data (Irwin et al. 2015) and predicts one interpretation of the current VLA and VLBA data. A relativistic jet model gives a good fit to both the current and original data (Lei et al. 2016), but suggests a rather different interpretation of the VLBA data. From this model, we estimated the initial Lorentz factor of the jet as $\Gamma_i \sim 10$ and a viewing angle of 40°. This off-axis viewing direction of the jet may explain its sub-Eddington luminosity (Nikolajuk & Walter 2013) as a result of a lower Doppler boosting factor. Furthermore, an extended (diameter ∼20 arcsec) disk component with spectral index $\alpha = 0.74$ ($F_\nu \propto \nu^{-\alpha}$) around the nucleus is shown in the radio data (Irwin et al. 2015), which is probably the counterpart of the soft X-ray excess and related to past star formation and/or SMBH activities.

2. Observations and Data Reduction

2.1. JVLA Observations

IGR J12580+0134 was observed five times within a period of 7 months with the VLA in 2011–2012 as part of the observations of NGC 4845 during the CHANG-ES program. These observations, which allowed the detection of the radio emission from the TDE 1–2 years from the event, were done at the L-band in the B, C , and D configurations, and in the C-band in the C and D configurations. At the L-band, the frequency coverage was (in GHz) 1.247 → 1.503 and 1.647 → 1.903 (500 MHz total); at the C-band it was 4.979 → 7.021 (2 GHz). The frequency gap at the L-band was set to avoid very strong persistent interference in that frequency range. The data and basic reduction procedures were previously discussed in Irwin et al. (2015), but here we detail additional work that was done subsequent to the analysis in that paper. Details of those observations are given in Table 1.

We observed IGR J12580+0134 with the JVLA in the A-configuration at the L-band (1.5 GHz) and C-band (5.5 GHz) on 2015 June 22 as part of program 15A-357. Both observations had a bandwidth of 1 GHz. Total integration times (over a single scan) were 129 and 479 s, respectively. The observations were done in full polarization mode (8-bit setups L16f2A and C16f2A), with 26 antennas. At both bands, 3C 286 was used to calibrate the flux scale and bandpass and J1224 +0330 was used to calibrate phase. For polarization calibration in both bands, 3C 286 was used to set the angle. Unfortunately, an unpolarized calibrator was not observed multiple times on 2015 June 22, which would have been needed for a proper correction of instrumental polarization. For the L-band, we used calibration scans on 3C 48 and 3C 84 from data set 15A-305 (PI Werner) taken on 2015 June 23. For this latter data set, 3C 48 was used as a bandpass calibrator before generating the d-terms from 3C 84. At the C-band, the leakage terms were set by a single observation of 3C 84 from project 15A-252 (PI Murphy) taken on 15 August 2015. The data reduction was conducted using CASA version 4.5.0 (release 35147). All data sets were Hanning smoothed and then inspected and flagged for RFI before a final calibration was applied following standard procedures.

At the L-band, after splitting off the source scan, we did a final flagging on the source scan and then imaged the data using CLEAN in multi-frequency synthesis (mfs) mode with nterms = 2, with a wide-field gridding mode and 1189 w-projection planes (calculated by CLEAN), and Briggs weighting (robust parameter 0.5). The image field was 2700″ square with 0.″25 pixels. The image shown in Figure 1 (top) was generated using CLEAN in psfmode CLARK after two rounds of phase-only self-calibration. However, to look for both linear and circular polarization, we also ran CLEAN on the original data set with psfmode CLARKSTOKES and nterms = 1. No significant signal was found in Q, U, or V. At the C-band, we proceeded similarly to the L-band data set, with an image size of 612″ square and 0.07″ pixels (beam size 0.″47×0.″33), an mfs mode with nterms = 2, with a wide-field gridding mode and 901 w-projection planes (calculated by CLEAN). The image shown in Figure 1 (bottom) is the I-only image after five rounds of phase-only self-calibration. Again, we also conducted a full stokes imaging (with nterms = 1) for the C-band data set but found no significant signal in Q, U, or V.

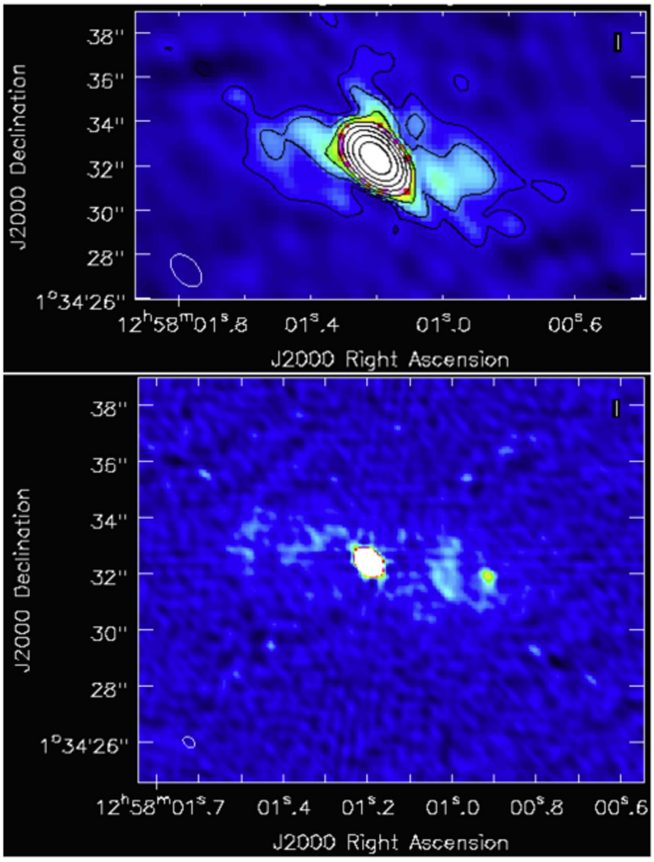

Figure 1. Images of the nuclear region of NGC 4845 from the JVLA in June 2015. In the top panel, we show the L-band observation, while in the bottom panel we show the C-band observation. Note that both images show extended emission that is likely associated with the galaxy's disk, as well as the nuclear component discussed in Section 3. The contours are at multiples of four times the off-source rms.

2.2. VLBA Observations

We observed IGR J12580+0134 with the]VLBA on 2015 October 8 (Table 1). Observations were done at 1.5 GHz (L-band) and 5.0 GHz (C-band), using the Roach Digital Back End and 8 IFs. Each IF is 32 MHz wide, and contains 128 × 250 kHz channels. All 10 antennas of the VLBA were used. The observations were done in full polarization mode, using 3C 286 to calibrate the JVLA's flux scale. J1254+0233 was used as a primary phase calibrator, and we used OQ208 as a D-term calibrator (all of these sources were observed on 8 October). Observations of NGC 4845 and J1254+0233 were grouped together in blocks of four (two at each frequency), with each individual scan on NGC 4845 lasting 4 minutes. Observations of OQ208 were done every 4th iteration, allowing coverage of more than 80° in parallactic angle, and the observations were phase-referenced, allowing for maximum sensitivity as well as absolute positional referencing. The total observing time was 5 hr, split evenly between the two bands. The data were correlated at the VLBA correlator in Socorro, New Mexico.

All data reductions for the VLBA observations were done in AIPS, following standard recipes in the AIPS Cookbook, specifically Appendix C.[12] We corrected for earth orientation, ionospheric conditions, and sampler errors using VLBAEOPS, VLBATECR, and VLBACCOR. Following this, we corrected for instrumental delays using VLBAPCOR and applied bandpass calibration in VLBABPSS. We then inspected the data in POSSM and did a priori amplitude calibration with VLBAAMP, using the gain and system temperature curves for each station, yielding correlated flux densities. Prior to fringe fitting, the supplied pulse calibration information was applied with the task PCCOR. Following this, the data were fringe-fit in VLBAFRNG. We also referenced the phases of NGC 4845 to those of J1254+0233. This allowed us to find absolute positional information for all the sources, as well as improve the sensitivity of the observations (see, e.g., Beasley & Conway 1995; Wrobel 2000). Because of some fairly severe interference at the L-band that could not easily be flagged out of the data, the phase-referencing was not successful in that band, and therefore we do not refer to absolute positions in that band. Parallactic angle and polarization calibration were done using VLBAPANG, using the OQ208 and 3C 286 observations. We followed the recommendation of the NRAO staff on polarization calibration[13], using 3C 286 to calibrate the position angles. Once these steps were done, the calibration was applied in SPLIT, which also yields single-source data files. To check the polarization calibration, we imaged J1254+0233 in both total flux and in polarization. No circular polarization was found.

Hybrid-mapping procedures were started using a point-source model for initial phase calibration. All images used ROBUST = 0 Briggs weighting (Briggs 1995). In subsequent iterations of self-calibration, we allowed first the phase and then both amplitude and phase to vary. We took care to ensure that each successive iteration of self-calibration did not go so deep as to start including negatives, residual side-lobes, or other spurious values, and that the peak specific intensity did not decline. In all, four iterations of phase-only self-calibration and two iterations of amplitude and phase self-calibration were done for the Stokes I images. All imaging and self-calibration were performed in AIPS, using the tasks IMAGR and CALIB, respectively, for the imaging/cleaning and self-calibration. Imaging of Stokes Q, U, and V were carried out using the self-calibration tables developed in the Stokes I imaging, combined with the polarization and D-term calibrators. We did not find significant emission in either Stokes Q or U. The circular polarization maps were made without fitting a spectrum across the band, because of the much smaller bandwidth of the VLBA data as compared to the JVLA data.

3. Results

The radio flux densities detected in our JVLA and VLBA observations are given in Table 2, along with the flux densities and in-band spectral indices. These include the values observed in 2011–2012 as part of the CHANG-ES survey (Irwin et al. 2015), as well as the 2015 JVLA imaging we report here. To compare with the CHANG-ES data reported in Irwin et al. (2015) and plotted in Figure 2, we define 2015 June 22 as T4, or T1+1270 days (times T1-T3 are defined in Irwin et al. 2015).

3.1. The AGN and Its Radio Variability

In the A-array observations we see evidence of a disk-like extension of diffuse emission, as previously seen in the earlier

[12] http://www.aips.nrao.edu/cook.html

[13] http://www.vla.nrao.edu/astro/calib/polar/

Table 2
Radio Interferometry Observations

Date	Config.	ν (GHz)	$I_{\rm tot}$ (mJy)	$I_{\rm peak}$ (mJy)	α	P (mJy)	V (mJy)	V/I (%)
1995 Feb 27	VLA/D (NVSS)	1.4	46.0 ± 1	...	...	...	...	...
1997 Aug 21, 25	VLA/C	8.4	12.5	...	...	...	...	...
1998 Oct 09	VLA/B (FIRST)	1.4351	33.9 ± 0.4	...	...	...	...	...
2011 Dec 19	VLA/D	6.00	432 ± 2	425 ± 3	...	2.3 ± 0.9	<0.036	$<8.3 \times 10^{-3}$
2011 Dec 30	VLA/D	1.57	230 ± 2	211 ± 3	...	0.55 ± 0.05	6.6 ± 0.2	2.9 ± 0.1
2012 Feb 23, 25	VLA/C	6.00	362 ± 1	355 ± 1	0.4 ± 0.2	<0.01	<0.01	$<2.8 \times 10^{-3}$
2012 Mar 30	VLA/C	1.57	260 ± 2	241 ± 3	...	0.35 ± 0.03	5.7 ± 0.1	2.2 ± 0.1
2012 Jun 11	VLA/B	1.57	238 ± 1	219 ± 4	...	1.2 ± 0.5	5.5 ± 0.4	2.3 ± 0.2
2015 Jun 22, 26	VLA/A	1.5195	118.0 ± 1.2	114.5 ± 0.7	0.54 ± 0.02	<0.12	<0.12	<0.1
2015 Jun 22, 26	VLA/A	5.499	36.32 ± 0.07	36.00 ± 0.04	1.25 ± 0.001	<0.03	<0.03	<0.1
2015 Oct 08	VLBA	1.5474	83.5[a] ± 1.1	65.9 ± 0.6	...[b]	<0.07	1.4 ± 0.2	1.7 ± 0.3
2015 Oct 08	VLBA	4.9795	29.9 ± 0.2	14.0 ± 0.1	...[b]	<0.06	<0.07	<0.2

Notes.
[a] Includes both core (72.7 ± 0.7 mJy) and fainter (northern) sources (10.8 ± 0.9 mJy).
[b] Band is too narrow for reliable fitting (Section 2.2).

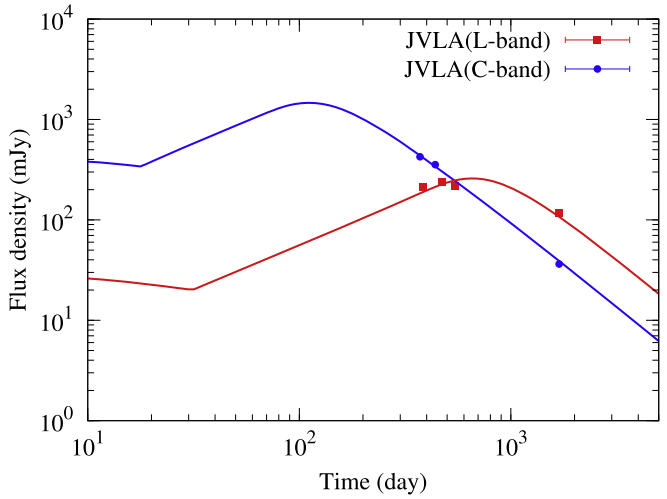

Figure 2. Radio light curves of the TDE, compared to a jet-CNM interaction model (Irwin et al. 2015; Lei et al. 2016), which predicts a power-law ($t^{-5/3}$) decay. Our data follow this very well, but note the importance of the 2015 data in obtaining the correct fit.

CHANG-ES data obtained with more compact configurations, although it is likely that some larger-scale structure is being resolved out at the A-configuration. We measured the flux of the central point source by fitting a Gaussian profile. At the L-band the resulting flux is 118 ± 1 mJy, with an in-band spectral index of $\alpha = 0.54 \pm 0.02$. At the C-band we measure 36.3 ± 0.1 mJy with an in-band spectral index of $\alpha = 1.25 \pm 0.03$. The error on the in-band spectral indices is dominated by errors in the flux model of the JVLA, as discussed in Perley & Butler (2013, 2017). The radio spectral index between the two bands is $\alpha = 0.90$, indicating significant spectral curvature between the bands.

Nearly five years from the initial event, it is clear that the radio source corresponding to the active nucleus (AGN) of NGC 4845 is still quite bright, albeit decreased significantly from that observed in late 2011, when flux densities ~250 mJy were observed. Multiple views of the light curve of the TDE are shown in Figure 2. Also looking at Table 2, it is obvious that the radio spectrum has evolved as a function of time, and the gigahertz peak seen in 2011–2012 has been replaced with a power law that steepens between 1 and 6 GHz. The radio spectrum has clearly evolved with time in the years since the 2010 November TDE. The 2015 JVLA and VLBA data are consistent with the presence of a spectral peak at frequencies below ~1 GHz, as predicted by the model, but we do not actually see any peak. While this is most likely due to a lack of lower-frequency observations, we cannot exclude the alternate possibility of multiple spectral components. We do not include the VLBA observations in Figure 2, as their resolution differs by nearly 3 orders of magnitude from that of the JVLA observations so that the flux densities are not comparable. This spectral evolution is shown in Figure 3. We discuss the evolution of the SED and its implications, in Section 4.2.

3.2. Parsec-scale Structure of the AGN

The central source of NGC 4845 was detected at both the L-band and C-band with the VLBA. We show the VLBA images in Figure 4. The VLBA images show two sources at the L-band, separated by 51.7 mas, translating to 4.1 pc projected distance. The main source is extended along the east–west direction, with the source being nearly 40 mas (3 pc) long and the flux maximum region being a broad plateau extending roughly southeast to northwest (Figure 4, bottom). Only one source is seen at the C-band, however. We fitted the flux maxima in both L-band and C-band images with elliptical Gaussians using JMFIT. The size and PA of these Gaussians were allowed to vary because of the extended nature of the central source in both images. The position of the C-band flux maximum is $\alpha = 12^{\rm h}58^{\rm m}01\overset{\rm s}{.}19814$, $\delta = 01°34'32\overset{''}{.}4203$, with internal 1σ errors (from JMFIT) of about 0.1 mas. The fitted component at the C-band had a maximum intensity of 9.80 ± 0.05 mJy/beam and a integrated intensity of 30.2 ± 0.2 mJy, with a deconvolved full-width at half-maximum of 2.8 ± 0.3 × 2.3 ± 0.2 mas in PA 128°. The fitted component at the L-band had a maximum intensity of 12.7 ± 0.1 mJy/beam and an integrated intensity of 60.1 ± 0.6 mJy, with a deconvolved full-width at half-maximum

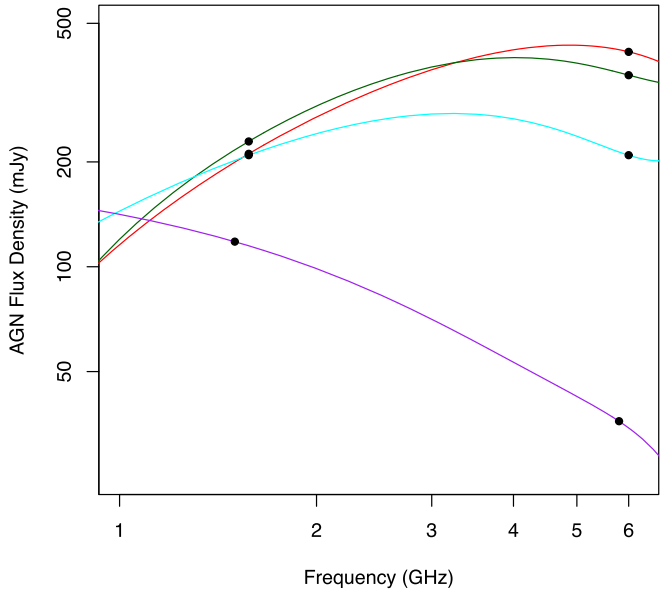

Figure 3. Radio spectra of the nuclear source (Table 2), along with polynomial fits, for four time stamps: T_1 (2011 December 30) in red, $T_2 = T_1 + 56$ days in green, $T_3 = T_1 + 196$ days in cyan, and $T_4 = T_1 + 1270$ days in purple. Note that not only has the radio spectrum between 1 and 6 GHz changed from being strongly inverted at epochs T_1 and T_2 to being flat at T_3 and steep at T_4, but also the position of the spectral peak has evolved, from ∼5 GHz at T_1 to ∼3.5 GHz at T_2 to <1 GHz at T_4. Note that the apparent spectral upturn of the fit to the T_4 data is most likely an artifact and not real: a power-law form (see the bottom panel) is much more likely.

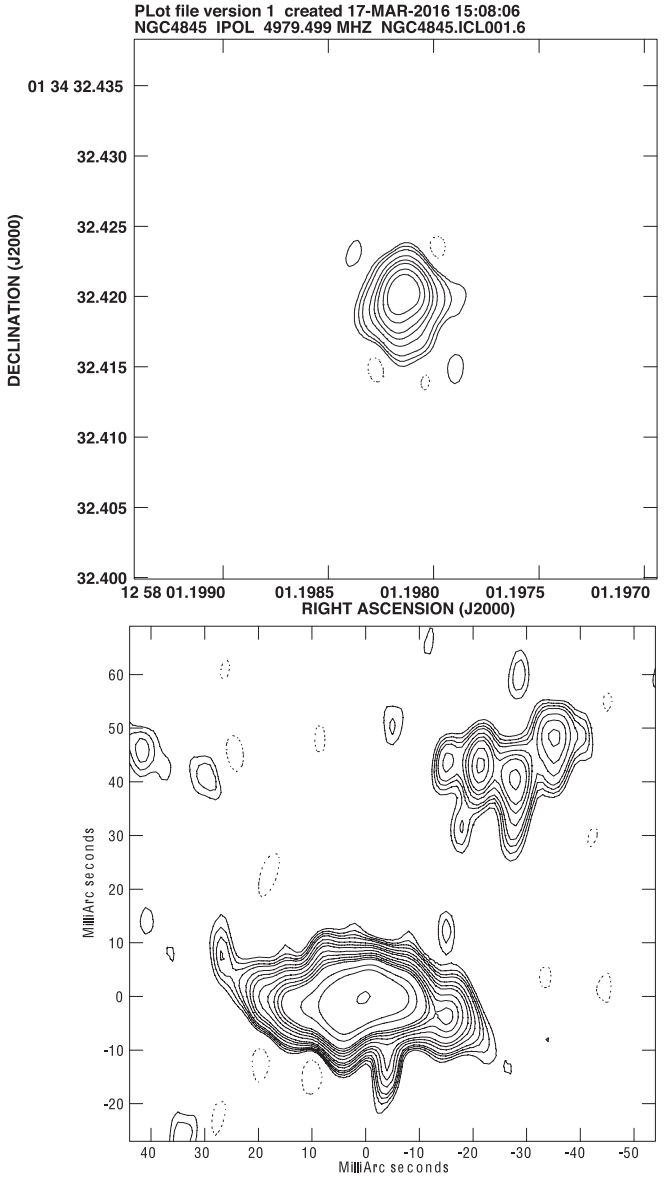

Figure 4. The nuclear region of NGC 4845, as seen in 2015 with the VLBA at (top) the C-band and (bottom) L-band. The contours in both panels are at (−3, 3, 5, 8, 16, 24, 32, 48, 64, 128, 256) times a base contour level of 0.1 mJy/beam. The rms noise of the image is given in Table 1. In the L-band, we have assumed that the position of the flux maximum is at (0, 0).

of $14.8 \pm 0.2 \times 5.6 \pm 0.3$ mas in PA 103°. Since JMFIT fits a Gaussian, the internal errors may be underestimates; however, they are consistent with the usual expectations of a few tenths of a pixel (the pixel size was 1 mas for the L-band VLBA image and 0.3 mas for the C-band VLBA image). The total flux of the southern VLBA source is 72.7 ± 0.7 mJy at 1.5 GHz and 29.9 ± 0.2 mJy at 4.9 GHz, while the northwest source, seen only at the L-band, has a flux of 10.8 ± 0.9 mJy. The total flux detected in the VLBA observations at the L-band is 71% of that seen in the JVLA observation, while the total flux detected by the VLBA at the C-band is 83% of that seen in the JVLA A-array data. It is thus apparent that the majority of the flux seen by the JVLA observations originated on milliarcsecond scales, although 20%–30% of that flux was resolved out and is on scales too large to be detected by the VLBA observations. Given the faintness of the source and the diffuse nature of the extended flux it is difficult to trust the outer contours too heavily, particularly given the interference in the L-band. However, the overall east–west nature of the central source and the resolved, northwest component survive all efforts to mask them out during cleaning.

While the spectral indices between the L-band and C-band are relatively easy to calculate in the JVLA data, the resolved nature of the VLBA structure means one needs to take additional steps. Using the entire VLBA source at both frequencies, without discriminating between the extended and unresolved components, one obtains $\alpha = 0.95$, broadly consistent with the 2015 JVLA interband spectral index. However, if instead we calculate a spectral index for the southern VLBI source, one obtains $\alpha = 0.81$ if one uses the entire flux measurement at the L-band, or $\alpha = 0.70$ using just the unresolved L-band flux. This is probably more indicative of the core, and roughly consistent with what is seen on arcsecond scales at epoch T_4 (Table 2 and Figure 3). While formally the VLBA data at the L-band cover over 300 MHz in bandwidth, in practice, for this faint of a source it proved impossible to fit a good spectral index value over any significant part of the image (for example the spectral index derived for the central source is 0.67 ± 0.59).

The northwest source is seen only at the L-band. We do not use the rms noise of the VLBA data to put an upper limit on its C-band flux, as that source is located more than 20 beam-widths away from the nuclear source. The task of detecting the northern source at the C-band is made even more difficult by its extended nature (Figure 3), spread over several beam-widths in the L-band data, with a significance peaking at just over 8σ in those data. The combination of those factors means that if the northwest source had $\alpha \approx 1$, a fairly steep spectrum typical of the mini-lobes seen in GPS sources (e.g., Snellen et al. 1999;

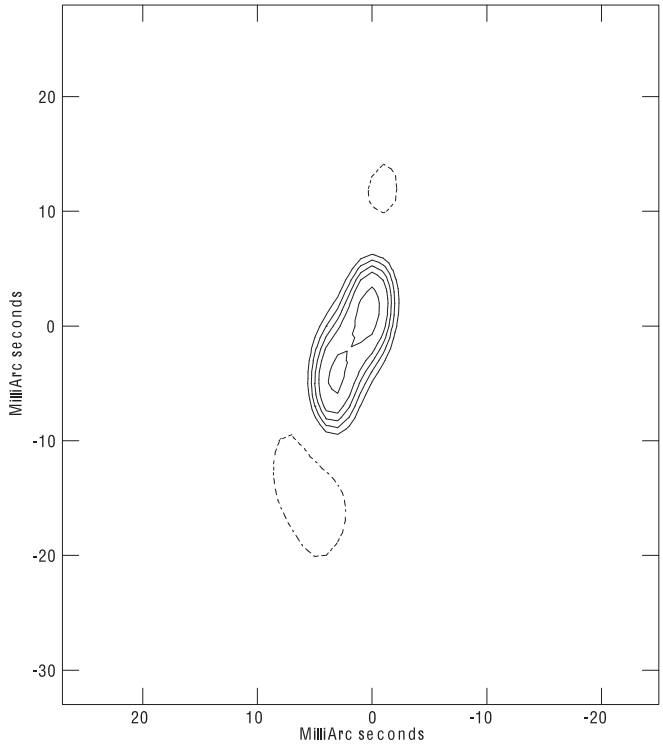

Figure 5. Nuclear region of NGC 4845, as seen in Stokes V in 2015 with the VLBA at the L-band. The contour levels are identical to Figure 4, and we have assumed the flux maximum is at (0, 0).

Tzioumis et al. 2002), it would be difficult or impossible to detect on our C-band VLBA image.

3.3. Polarized Emission

A very interesting property of the radio source is its circular polarization, first noted in the early CHANG-ES observations by Irwin et al. (2015). As shown in Table 2, our VLBA observations reveal a significant ($\sim 10\sigma$) detection of circular polarization in the L-band, while no circular polarization is seen in the JVLA data or at the C-band in the VLBA observations. We do not detect any significant linear polarization in any of our images (Table 2). We show an image of the circular polarization (Stokes V) in Figure 5. As seen, the circularly polarized emission in the L-band is resolved, but given the fact that it lies southeast of the higher frequency, the C-band flux maximum (see Figures 4 and 5), which in AGNs is usually interpreted as more indicative of the location of the nucleus, its apparent alignment with the position angle between the central and NW source is likely an illusion.

We used JMFIT to measure the flux and extent of this component. The resolved component has a size of $11.0 \pm 0.7 \times 4.5 \pm 0.3$ mas in PA 162°. However, due to the low flux of the component, JMFIT was not able to converge well on a deconvolved size for this component, obtaining $6.7 \pm 1.6 \times 0.0 \pm 0.5$ mas in PA 138°. As can be seen, the level of circular polarization in our 2015 VLBA data is somewhat decreased from the ~3% values seen in L-band epochs $T_1 - T_3$. We further discuss the evolution and nature of the polarization in Section 4.4.

4. Discussion

The disruption of a star or substellar object by tidal forces in the neighborhood of a galaxy's SMBH is an exciting event that has broad-ranging implications. Large amounts of material can be injected into the accretion flow surrounding the black hole, and if the previous rate of accretion was small, an inactive black hole can become active—and in the process, exhibit some of the same properties as viewed in other, less transient AGN classes. However, not all AGN properties may be exhibited in a TDE. The properties seen may depend on the exact physical conditions during the TDE as well as the nuclear environment. However, there are a few unambiguous detections in the radio of a compact source connected with a TDE. Zauderer et al. (2011) reported JVLA observations of the TDE Swift J1644+57. That source, further analyzed by Berger et al. (2012) and Zauderer et al. (2013), appeared to occur in a fairly pristine galactic environment, and appeared to decline precipitously in brightness after several hundred days. The later "core shutoff" (Zauderer et al. 2013) has also likely occurred for IGR12580+0134 (Nikolajuk & Walter 2013). Swift J1644+57 was also observed by the EVN (Yang et al. 2016), which found a compact radio source but no evidence for superluminal motion.

Romero-Cañizales et al. (2016) claimed the detection of a compact milliarcsecond nuclear source in the TDE ASASSN-14li. It was hosted in the post-starburst galaxy PGC 04324 ($d = 90$ Mpc), and the radio source they identify is far fainter (~1 mJy at the L-band, compared to over 60 mJy in our observations). Thus the nuclear source we detect in IGR12580 +0134 is over a factor of 2 more powerful and our constraints on its size (using the C-band FWHM) are a factor of 6 smaller—corresponding to a projected linear size of <0.16 pc, although we caution the reader that the nuclear source is resolved. Thus, while future, higher-frequency observations can constrain this size further, we can say that the observed radio structure is not consistent with non-relativistic, spherical expansion of the disrupted object's remains. An alternative scenario that might produce a roughly spherical source is the scattering of the high-energy radiation from the TDE by nuclear dust. Lu et al. (2016) showed that this could produce significant near-infrared and mid-infrared emission for months to years after the event. Thought this is a possibly exciting prospect for *JWST*, such emission would be undetectable in the radio. Also unlikely, for similar reasons (plus the fact that a bright flare of a factor of 10 would be difficult to explain) is a bright source connected with the Pa α emission from the nuclear mini-spiral, discussed by Wang et al. (2010). In this section, we discuss the implications of our findings, both in terms of the nature of the milliarcsecond resolved component and its evolution, as well as the evolution of the broadband radio spectrum and the source polarization.

4.1. Nature and Evolution of the Milliarcsecond Scale Emission

The discovery of a resolved component in VLBA imaging of IGR J12580+0134 is exciting, and the implications of such a discovery deserve a full discussion. There are two possibilities. The first is that the northwest component is unassociated with the TDE. We consider this possibility (which we consider more likely) at the end of this section. However, an alternate, more exciting possibility needs to be considered. If one assumes that the northwestern source constitutes material ejected during the

TDE in a relativistic flow, the average implied speed of the component is $\beta_{\rm app} = 2.4c$. This value of $\beta_{\rm app}$ is not inconsistent with the estimate of viewing angle $\theta = 40°$ from Lei et al. (2016), which would indicate an ejection velocity of $0.96c$ and a bulk Lorentz factor $\Gamma = 3.6$. At one level, this scenario seems likely, and the morphology of the NW VLBA source is suggestive of an expanding source at the working surface of a conical outflow. The implied bulk Lorentz factor is significantly lower than the $\Gamma = 10$ assumed in the model of Lei et al. (2016). This is not problematic. The combination of β and θ is not robustly constrained, and in addition, if the jet is interacting with a sufficiently dense CNM, it is very likely that its working surface would decelerate as a function of time (see Section 4.2)

However, we believe it is most likely that the northwest component is not connected with the 2010 November TDE, because (as we detail in Section 4.2) we consider it likely that the interaction of the jet with the dense CNM produced significant deceleration in the jet within the first year. Such an interpretation (which will be tested by second-epoch VLBA observations in Spring 2017) is also suggested by the orientation of the extension to the circularly polarized L-band source, which (taking the point closest to the C-band nucleus as "upstream") points *away* from the northwest source. This is not the first resolved component seen in a TDE. Romero-Cañizales et al. (2016) also claimed the detection of a fainter (0.1 mJy), possibly elongated companion source 4.3 mas (1.9 pc projected distance) from the nuclear source of ASSASN-14li. That component, like the northwest source here, could either be a jet component related to the TDE, the remnant of a previous TDE event, or a binary black hole.

If the northwest component is unrelated to the 2010 TDE, it could either be a remnant of an earlier TDE event or a supernova remnant of luminosity $\sim 10^{27}$ erg s^{-1} Hz^{-1} (given the resolved nature of the northwest component, a binary black hole origin is extremely unlikely). While uncommon, that is not exceptional for supernova remnants in nearby galaxies (see, e.g., the discussion and luminosity functions in Chomiuk & Wilcots 2009). Moreover, this latter interpretation is consistent with the fact that NGC 4845, the host of this TDE, is a dusty, spiral galaxy that hosts a LINER (Spinoglio & Malkan 1989), and perhaps also active star formation in its center. It could also be a smaller-scale counterpart to the large-scale disk seen on the JVLA images, although this seems less likely, as such a high surface brightness feature (total extended flux in the L-band is greater than the unresolved component) would be difficult to reconcile with the low activity state of the nuclear black hole prior to the TDE. More likely is a SNR origin, although the FIRST and NVSS fluxes set an upper limit on the flux from SNRs.

4.2. A Model for the Expanding Nuclear Structure

On a more detailed level, the physical picture of the jet evolution in the CNM is similar to that of GRBs, except for an off-axis viewing angle correction (Granot et al. 2002). The central engine, the tidal disruption of stellar objects by SMBHs, powers relativistic jets, which then propagate in the CNM. Shocks can be produced via the the jet-CNM collision, and high-energy electrons can be accelerated. The synchrotron and/or inverse Compton emission of accelerated electrons gives the multi-wavelength afterglow emission.

Here we model the possible evolution of the ejecta. The evolution of the jet can be roughly divided into three stages, the coasting phase, the deceleration phase, and the Newtonian phase. Its dynamics is governed by a set of hydrodynamical equations (Huang et al. 2000). We solve the dynamics of the forward shock numerically, and calculate the synchrotron emission from the accelerated electrons (Sari et al. 1998). The parameters of the model include the launching time, energetics, initial Lorentz factor, opening angle, electron, and magnetic energy partition of the jet, the spectral index of accelerated electrons, the viewing angle, and the CNM density (see Table 3). We assume an instantaneous injection of energy into the jet.

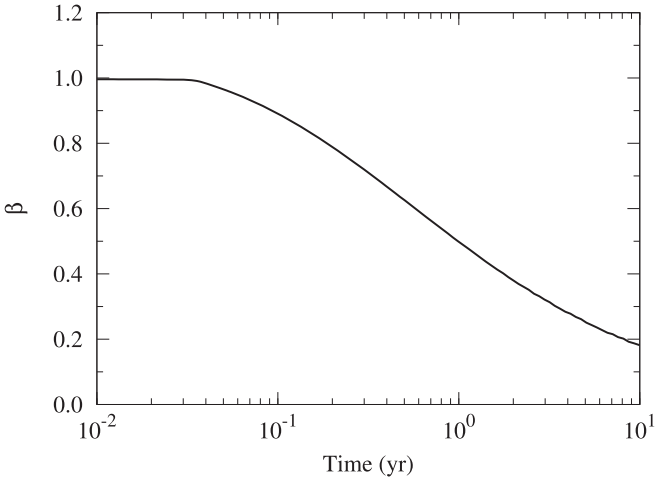

Figure 6. Evolution of the velocity of the jet with time in the observer's frame.

The evolution of the jet velocity is shown in Figure 6. The deceleration time of the jet can be estimated as

$$t_{\rm dec} = a_{\rm off}^{-1}(1+z)\left[\frac{3E_k}{16\pi n m_p \Gamma^8 c^5}\right]^{1/3} \simeq 0.13\, a_{\rm off}^{-1} n^{-1/3} E_{50}^{1/3} \Gamma_1^{-8/3}\ {\rm days}, \quad (1)$$

where $E_{50} = E_k/10^{50}$ erg, $\Gamma_1 = \Gamma/10$. The off-axis factor $a_{\rm off}$ is defined as the ratio of the off- to on-axis Doppler factor, $a_{\rm off} = (1-\beta)/(1-\beta\cos\psi)$, with β being the velocity of the jet in units of light speed, and $\psi = \max(\theta_{\rm obs} - \theta_j, 0)$ being the angle between the jet moving direction and the line of sight. For the parameters given in Table 3, $t_{\rm dec} \sim 10$ day. The integral distance traveled by the jet is about 0.4 pc, which is much smaller than the separation between the northwest and southeast sources ($\sim$4.1 pc). This is roughly consistent with the size of the circularly polarized component (Figure 5). The average implied speed of the ejecta over five years would then be $\sim 0.3c$.

Other TDEs have also had models published for subluminally modeled components. The upper limit published by Yang et al. (2016) for the average velocity of Sw 1644+57's ejecta was similar to ours. Alexander et al. (2016) modeled a subluminally moving component in ASSASN-14li that could be traced back to the TDE itself, using the radio spectrum alone. The possibility of significant unbound matter (perhaps as much as half of the original mass of the disrupted object) was discussed by Krolik et al. (2016), who pointed out that if left undisturbed the material would coast outward from the black hole at a speed $\sim [GM_{\rm BH}/a_{\rm min}]^{1/2}$, where $a_{\rm min}$ is the semimajor axis of the disrupted object's original orbit. And,

Table 3
Model Parameters

Jet Launching Time Δt (day)	CNM Density n (cm^{-3})	Viewing Angle θ_{obs} (degree)	Jet KE E_{50}[a]	Initial Γ_j	Initial θ_j (degree)	p[b]	ϵ_e[c]	ϵ_B[c]
18[d]	1.2	35	530	11.2	3.7	2.70	0.21	0.05

Notes.
[a] In 10^{50} erg s^{-1}.
[b] Spectral index of accelerated electrons.
[c] Fraction of the ejecta kinetic energy assigned to accelerated electrons or the magnetic field.
[d] Relative to 2010 December 12.

interestingly, Giannios & Metzger (2011) and Mimica et al. (2015) have published a model for Sw 1644+57 that includes an ultrarelativistic core (Lorentz factor $\Gamma \sim 10$) surrounded by a slower ($\Gamma \sim 2$) sheath that provides a reasonable fit to that TDE's light curve. That model also would fit the light curve of IGR 12580+0134, but in NGC 4845's nuclear environment it would likely be subject to the same deceleration that we discuss above.

4.3. Evolution of the Circumstellar Medium and Broadband Spectrum

Lei et al. (2016) and Irwin et al. (2015) fitted the early VLA data with a jet-CNM interaction model that assumes a conically expanding, synchrotron-emitting jet source that is initially optically thick due to synchrotron self-absorption at gigahertz frequencies, with an optical thickness that changes as a function of time, likely as a result of the expansion of the jet. The model assumed an initial Lorentz factor of the jet as $\Gamma_i \sim 10$ and a viewing angle of 40°. Figure 7 shows the spectral energy distributions (SEDs) for a joint fitting to the VLA observations at four epochs, T_1 (2011 December 30), $T_2 = T_1 + 56$ days, $T_3 = T_1 + 196$ days, and $T_4 = T_1 + 1270$ days (Irwin et al. 2015), as well as the *PLANCK* observations at $T_0 = T_1 - 348$ days (Yuan et al. 2016). Model parameters are given in Table 3.

The flux densities at different epochs can be well described by the model. The decline in the source flux follows the $t^{-5/3}$ behavior predicted by Irwin et al. (2015), their Equation (22)). Earlier observations showed that the spectrum peaked between the L-band and C-band, with the peak shifting to lower frequencies with time (Irwin et al. 2015). We now see a continuation of that spectral trend, i.e., that the peak of the spectrum has shifted to a frequency below the L-band. Note also that the shape of the radio through IR SED rules out a significant thermal contribution except at epoch T_0 when the submillimeter upturn in the *Planck* data could be explained by thermal dust emission from a torus, perhaps heated by the TDE. This would also be reasonable given its classification as a LINER (Spinoglio & Malkan 1989).

Figure 8 shows the comparison of the in-band spectral indices between the measurements and the model prediction. We find that the model prediction can roughly reproduce the evolution trend (i.e., from hard to soft) of the spectra. However, quantitatively there are discrepancies between these two. Some of this is due to the details of the model (shock strength, injection index, and Mach number, for example). In addition, at the L-band, the emission is significantly affected by the self-absorption of the synchrotron emission, which makes the estimate of the spectral indices inaccurate. At the C-band, however, the emission is expected to be optically thin, and the evolution of α may indicate spectral variations of the accelerated electrons during the jet propagation.

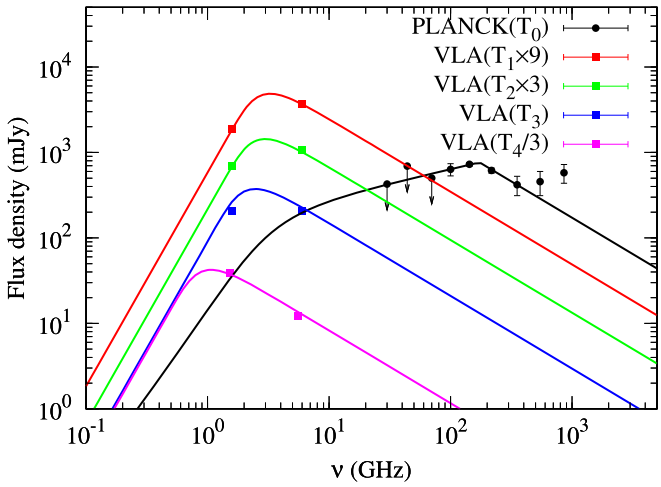

Figure 7. SEDs of the jet emission from JVLA observations at the L-band (∼1.54 GHz) and C-band (∼5.75 GHz), and observed by *Planck* at $T_0 = T_1 - 348$ days (Yuan et al. 2016), and by VLA at T_1, T_2, T_3, and T_4. For visual clarity, the SEDs have been vertically offset, as indicated in the legend. Lines show the model fitting results. See Section 4.2 for details.

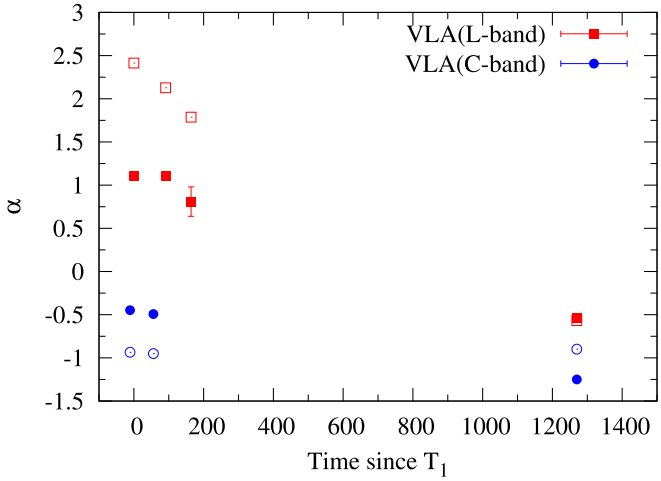

Figure 8. In-band spectral indices of the TDE, from the VLA measurements (filled symbols) at the L-band and C-band, compared with that expected from the jet-CNM model (open symbols).

4.4. Interpretation of the Circular Polarization

The lack of detection of circular polarization at the C-band in our VLBA data is consistent with the earlier JVLA observations from Irwin et al. (2015). Those authors explained the circular polarization observed as due to conversion from linear polarization to circular polarization via generalized Faraday rotation (see also Beckert & Falcke 2002; O'Sullivan et al. 2013). The decrease of the circular polarization at the L-band over five years could then be explained via a gradually decreasing Faraday depth, consistent with the declining optical depth that explains the gradual spectral evolution shown in Figure 3. A closer look at Figure 3 shows that not only has the source spectrum has taken on a much more power-law type shape over the intervening five years since epoch T_1, but in fact, as discussed in Section 3.1, this indicates a low optical depth for the source at epochs T_4 and later on large scales including the time of our JVLA observation. In that case, we would not expect to see a significant circular polarization. However, on small scales it might still be possible to see small optically thick portions in the 2015 VLBA observations. We regard this as more likely than the alternate explanation of variability for the lack of arcsecond-scale circular polarization in the 2015 JVLA observations. While plausible, as Hovatta et al. (2012) and Homan & Lister (2006) have pointed out that circular and linear polarization vary commonly for MOJAVE blazars, it does require additional complexity and therefore Occam's razor argues against it. We note that the C-band flux maximum lies at the northern end of the circularly polarized region in the L-band. If indeed the C-band flux comes predominantly from downstream of the L-band flux maximum then the C-band emitting region has an inverted and optically thin spectrum more similar to many VLBI cores. The future development of this region will be interesting to watch.

4.5. Conclusions

The TDE IGRJ 1258+0134 is now seen to have a complex radio structure on milliarcsecond scales that is most likely connected to the TDE. The radio spectrum displays a complex evolution that, while broadly consistent with earlier modeling of this source, is much better defined with the addition of these data. The nature of the parsec-scale structure is both unclear. While the observed northwest component could be evidence of a superluminally moving component ejected as part of the cosmic microwave background, we believe this is unlikely, as modeling suggests that due to the dense nuclear ICM the jet should decelerate on timescales of months and have a much smaller, subparsec size, more consistent with the size of the circularly polarized component observed at the L-band.

This work is based on observations made with the Karl G. Jansky Very Large Array (JVLA) and the Very Long Baseline array (VLBA). We acknowledge an interesting conversation with Sjoert Van Velzen about this paper.

References

Alexander, K. D., Berger, E., Guillochon, J., Zauderer, B. A., & Williams, P. K. G. 2016, ApJL, 819, L25
Beasley, A. J., & Conway, J. E. 1995, in ASP Conf. Ser. 82, Very Long Baseline Interferometry and the VLBA, ed. J. A. Zensus, P. J. Diamond, & P. J. Napier (San Francisco, CA: ASP), 327
Beckert, T., & Falcke, H. 2002, A&A, 388, 1106
Berger, E., Zauderer, A., Pooley, G. G., et al. 2012, ApJ, 748, 36
Bloom, J., Giannios, D., Metzger, B. D., et al. 2011, Sci, 333, 203
Briggs, D. 1995, PhD Thesis, New Mexico Institute of Mining & Technology
Burrows, D., Kennea, J. A., Ghisellini, G., et al. 2011, Natur, 476, 421
Cenko, S., Krimm, H. A., Horesh, A., et al. 2012, ApJ, 753, 77
Chen, X., Madau, P., Sesana, A., & Liu, F. K. 2009, ApJL, 697, L149
Chomiuk, L., & Wilcots, E. M. 2009, AJ, 137, 3869
Giannios, D., & Metzger, B. D. 2011, MNRAS, 416, 2102
Granot, J., Panaitescu, A., Kumar, P., & Woosley, S. E. 2002, ApJL, 570, L61
Homan, D. C., & Lister, M. L. 2006, AJ, 131, 1261
Hovatta, T., Lister, M. L., Aller, M. F., et al. 2012, AJ, 144, 105
Huang, Y. F., Gou, L. J., Dai, Z. G., & Lu, T. 2000, ApJ, 543, 90
Irwin, J., Henriksen, R. N., Krause, M., et al. 2015, ApJ, 809, 172
Krolik, J., Piran, T., Svirski, G., & Cheng, R. M. 2016, ApJ, 827, 127
Lei, W., Yuan, Q., Zhang, B., Wang, D., et al. 2016, ApJ, 816, 20
Levan, A. J., Tanvir, N. R., Cenko, S. B., et al. 2011, Sci, 333, 199
Lu, W., Kumar, P., & Evans, N. J. 2016, MNRAS, 458, 575
Magorrian, J., & Tremaine, S. 1999, MNRAS, 309, 447
Mimica, P., Giannios, D., Metzger, B. D., & Aloy, M. A. 2015, MNRAS, 450, 2824
Nikolajuk, M., & Walter, R. 2013, A&A, 552, A75
O'Sullivan, S. P., McClure-Griffiths, N. M., Feain, I. J., et al. 2013, MNRAS, 435, 311
Perley, R. A., & Butler, B. J. 2013, ApJS, 204, 19
Perley, R. A., & Butler, B. J. 2017, ApJS, 230, 7
Phinney, E. 1989, in IAU Symp. 136, The Center of the Galaxy, ed. M. Morris (Kluwer: Dordrecht), 543
Romero-Cañizales, C., Prieto, J. L., Chen, X., et al. 2016, ApJL, 832, L10
Sari, R., Piran, T., & Narayan, R. 1998, ApJL, 497, L17
Snellen, I. A. G., Schilizzi, R. T., Miley, G. K., et al. 1999, NewAR, 43, 675
Spinoglio, L., & Malkan, M. A. 1989, ApJ, 342, 83
Tzioumis, A., King, E., Morganti, R., et al. 2002, A&A, 392, 841
Walter, R., Bordas, P., Bozzo, E., et al. 2011, ATel, 3108, 1
Wang, J., & Merritt, D. 2004, ApJ, 600, 149
Wang, Q. D., Dong, H., Cotera, A., et al. 2010, MNRAS, 402, 895
Wrobel, J. M. 2000, ApJ, 531, 716
Yang, J., Paragi, Z., van der Horst, A. J., et al. 2016, MNRAS, 462, L66
Yuan, Q., Wang, Q. D., Lei, W.-H., Gao, H., & Zhang, B. 2016, MNRAS, 461, 3375
Zauderer, B. A., Berger, E., Margutti, R., et al. 2013, ApJ, 767, 152
Zauderer, B. A., Berger, E., Soderberg, A. M., et al. 2011, Natur, 476, 425